



1 **SEAMUS (v1.0): a $\Delta^{14}\text{C}$ -enabled, single-specimen sediment accumulation simulator**

2 Bryan C. Lougheed^{1,2}

3 1. Department of Earth Sciences, Uppsala University, Uppsala, Sweden.

4 2. Laboratoire d'Océanologie et de Géosciences, Université du Littoral Côte d'Opale, Wimereux,
5 France.

6 Corresponding author: B.C. Lougheed (bryan.lougheed@geo.uu.se)

7 **Abstract**

8 The systematic bioturbation of single particles (such as foraminifera) within deep-sea sediment
9 archives leads to the apparent smoothing of any temporal signal as record by the downcore,
10 discrete-depth mean signal. This smoothing is the result of the systematic mixing of particles from a
11 wide range of depositional ages into the same discrete depth interval. Previous sediment models
12 that simulate bioturbation have specifically produced an output in the form of a downcore, discrete-
13 depth mean signal. Palaeoceanographers analysing the distribution of single foraminifera specimens
14 from sediment core intervals would be assisted by a model that specifically evaluates the effect of
15 bioturbation upon single specimen populations. Taking advantage of recent increases in computer
16 memory, the single-specimen SEDiment AccuMulation Simulator (SEAMUS) was created in Matlab,
17 whereby large arrays of single specimens are simulated. This simulation allows researchers to
18 analyse the post-bioturbation age heterogeneity of single specimens contained within discrete-
19 depth sediment core intervals, and how this heterogeneity is influenced by changes in sediment
20 accumulation rate (SAR), bioturbation depth (BD) and species abundance. The simulation also
21 assigns a realistic ^{14}C activity to each specimen, by considering the dynamic $\Delta^{14}\text{C}$ history of the Earth
22 and temporal changes in reservoir age. This approach allows for the quantification of possible
23 significant artefacts arising when ^{14}C dating multi-specimen samples with heterogeneous ^{14}C activity.
24 Users may also assign additional desired carrier signals to specimens (e.g., stable isotopes, trace
25 elements, temperature, etc.) and consider a second species with an independent abundance. Finally,
26 the model can simulate a virtual palaeoceanographer by randomly picking whole specimens
27 (whereby the user can set the percentage of older, 'broken' specimens) of a prescribed sample size
28 from discrete depths, after which virtual laboratory ^{14}C dating and ^{14}C calibration is carried out
29 within the model.



30 **1.0 Introduction**

31 Deep-sea sediment archives provide valuable insight into past changes in ocean circulation and
32 global climate. The most often studied carrier vessels of the climate signal are the calcite tests of
33 foraminifera. The tests of these organisms incorporate isotopes and trace elements of the ambient
34 water at the time of calcification, before sinking to the seafloor sediment archive after death. Each
35 discrete-depth interval of a sediment core (typically 1 cm core slices) retrieved from the sea floor
36 can contain many thousands of specimens. Researchers have typically had to combine many tens or
37 hundreds of single tests into a single sample for successful analysis using mass spectrometry.
38 Furthermore, post-depositional sediment mixing (e.g. bioturbation (Berger and Heath, 1968)) of
39 deep-sea sediment means that foraminifera specimens of vastly differing ages can be mixed into the
40 same discrete-depth interval. The main consequence of this mixing is that a downcore, discrete-
41 depth multi-specimen reconstruction of a specific climate proxy will appear to be strongly smoothed
42 out (on the order of multiple centuries or millennia) when compared to the original temporal signal
43 (Pisias, 1983; Schiffelbein, 1984; Bard et al., 1987). Moreover, machine analysis of multi-specimen
44 samples will only report the mean value and machine error, thus hiding the true distribution of
45 values within the sample. Advances in mass spectrometry eventually allowed the analysis of single
46 specimens (Killingley et al., 1981) and, since single specimens capture a single year/season of the
47 climate signal, researchers can study the full distribution of isotope or trace element values obtained
48 from single specimens contained within various discrete depths of sediment cores to make
49 inferences regarding variability in climate, habitat or specimen morphology for various specific time
50 periods during the Earth's history (Spero and Williams, 1990; Tang and Stott, 1993; Billups and
51 Spero, 1996; Ganssen et al., 2011; Wit et al., 2013; Ford et al., 2015; Metcalfe et al., 2015, 2019b;
52 Ford and Ravelo, 2019). However, the accuracy with which the aforementioned studies can quantify
53 time-specific variation for a particular climate period, habitat or morphological variable is strongly
54 dependent upon the constraint of the age range of the specimens contained within a given discrete-
55 depth interval. The aforementioned studies still rely strongly upon the mean depth age method to
56 assign an age range to all specimens contained within a discrete depth interval, and previous models
57 of single specimen analysis in sediment cores do not include bioturbation (Thirumalai et al., 2013;
58 Fraass and Lowery, 2017). Such an approach can be problematic if, to give but one example, an
59 assumed Holocene age 1-cm slice of sediment core were to also contain a significant number of Late
60 Glacial specimens, which could lead to a spurious interpretation of Holocene climate variability.
61 Ultimately, this problem can be circumvented through the application of paired analysis of both
62 radiocarbon (^{14}C) and stable isotopes on single specimens (Lougheed et al., 2018), but the current
63 mass requirements of ^{14}C accelerated mass spectrometry (AMS) means that such a method is



64 currently limited to very large specimens (>100 μg), whereas most planktonic foraminifera used in
65 palaeoceanography are of an order of magnitude smaller. Until such time that single specimen ^{14}C
66 methods become systematically applicable to planktonic specimens, and for periods older than the
67 analytical limit of ^{14}C dating (>50 ka), a sediment accumulation model specifically designed for the
68 analysis of single specimens can help shed light on the age distributions planktonic foraminifera
69 contained within discrete depths.

70 Using a model to quantify the distribution of specimen ages within discrete-depth sediment intervals
71 is also important for ^{14}C dating applied to multi-specimen samples, which can be expected to have
72 heterogeneous radiocarbon (^{14}C) activity. This heterogeneity is governed by the Earth's dynamic $\Delta^{14}\text{C}$
73 history, temporal changes in species abundance, sediment accumulation rate (SAR) and in local ^{14}C
74 reservoir age. Temporal changes in ^{14}C heterogeneity have the potential to induce downcore age-
75 depth artefacts when ^{14}C analysis and ^{14}C calibration are applied to multi-specimen samples. The
76 ability to make a quantitative estimate of downcore changes in the ^{14}C heterogeneity and its effect
77 upon ^{14}C dating would help to improve Late Glacial and Holocene geochronologies for deep-sea
78 sediment archives.

79 Here, the $\Delta^{14}\text{C}$ -enabled single-specimen SEdiment AccuMulation Simulator (SEAMUS) is presented.
80 This model takes advantage of advances in computing power to simulate a large array of single
81 specimens. Such an approach allows for a relatively straightforward execution of transient runs with
82 temporally dynamic time series inputs for sediment accumulation rate (SAR), species abundance,
83 bioturbation depth (BD), ^{14}C reservoir age, $\Delta^{14}\text{C}$ and any desired carrier signal(s). Single specimen
84 populations are essentially transferred from the time domain to the depth domain, thus simulating
85 the sedimentation history of the resulting sediment archive. The distribution of discrete depth single
86 specimen true age, ^{14}C activity, bioturbation history (number of bioturbation cycles), and carrier
87 signal can subsequently be investigated and relationships with the dynamic input parameters can be
88 explored. Subsequently, users can subject the simulated sediment archive to a picking procedure
89 (with a prescribed number of randomly picked whole specimens per sample) to create virtual
90 subsamples from each discrete core depth, whereby one can also consider the presence of broken
91 (non-picked) specimens, which have been through more bioturbation cycles and are therefore older.
92 From these virtual subsamples, mean carrier signal values and species abundances can be calculated,
93 allowing users to evaluate their downcore core reconstructions for the possible presence of
94 artefacts. Furthermore, these virtual subsamples can be used to calculate virtual laboratory ^{14}C
95 dates, which are subsequently calibrated using the *MatCal* (Lougheed and Obrochta, 2016)
96 calibration software. Calibrated age distributions for a discrete depth can be compared to their



97 associated simulated true age distribution, thus evaluating the accuracy of the ^{14}C dating and
98 calibration process.

99 **2.0 Model description**

100 **2.1 Bioturbation understanding and previous models**

101 The most commonly used mathematical model of bioturbation in deep-sea sediments is the so-
102 called Berger-Heath bioturbation model, which assumes a uniform an instantaneous (on geological
103 timescales) mixing of the bioturbation depth (BD), the uppermost portion of a sediment archive
104 where oxygen availability allows for the active bioturbation of sediments (Berger and Heath, 1968;
105 Berger and Johnson, 1978; Berger and Killingley, 1982). Observations of uniform mean age in the
106 uppermost intervals of sediment archives do indeed support this mixing model (Peng et al., 1979;
107 Boudreau, 1998), and the BD itself has been shown to be related to the organic carbon flux at the
108 seafloor (Trauth et al., 1997). Researchers wishing to carry out transient bioturbation simulations
109 with dynamic input parameters have incorporated the Berger-Heath mathematical model into their
110 computer models to, most notably the FORTRAN77 model TURBO (Trauth, 1998), its updated
111 MATLAB version TURBO2 (Trauth, 2013) and the more recent R model Sedproxy (Dolman and
112 Laepple, 2018). In the case of TURBO2, the user inputs a number of idealised, non-bioturbated
113 stratigraphical levels with assigned age, depth, carrier signal and abundance. Subsequently, TURBO2
114 outputs the bioturbated carrier signal and abundance values corresponding to the inputted
115 stratigraphic levels. Consequently, TURBO2 is of most interest for researchers who would like to
116 understand the perturbation of the mean downcore signal. Sedproxy allows the user to input a
117 climate data in the time domain, along with sediment core variables (such as SAR and BD), after
118 which mathematical computations are used to produce the equivalent bioturbated climate data also
119 in the time domain, whereby single specimen distributions can also be quasi-inferred.

120 **2.2 The SEAMUS model**

121 **2.2.1 Short description of the model**

122 The SEAMUS simulation is an iterative model that actively simulates the sedimentation process of
123 single specimens on a per timestep basis, whereby input data in the time domain is converted into
124 the core depth domain. For each timestep, a number of new specimens are added to the top of the
125 simulated core, with bioturbation subsequently being carried out. SEAMUS uses the sediment core
126 and species abundance variables inputted in the time domain (SAR in the form of an age-depth
127 model, BD vs time, species abundance vs time) to simulate a number of new single specimens per
128 timestep. Each of these specimens are assigned an age, ^{14}C activity, reservoir age and carrier signal



129 corresponding to the timestep. Subsequently, the new specimens are added to the top of the
130 existing core, after which bioturbation is carried out. The simulation takes advantage of recent
131 increases in computer memory capacity to keep track of the depths, ages, ^{14}C activities, species
132 types and number of bioturbation cycles for all single specimens in the simulation. Such an
133 approach, which is optimised for single specimens, allows the user to use logical indexing to quickly
134 access all variables for given single specimens for given depths, ages and/or species.

135 The SEAMUS simulation is broken down into two main functions that the user can call. The first
136 function *seamus_run*, carries out the actual single specimen sedimentation simulation based on the
137 input parameters designated by the user. The second function, *seamus_pick*, can be best described
138 as a ‘virtual palaeoceanographer’, in that it carries out downcore analysis of the simulated sediment
139 core, including discrete-depth sample picking, calculation of sub-sample mean carrier signals, ^{14}C
140 analysis by virtual AMS, ^{14}C calibration, etc. The *seamus_run* and *seamus_pick* functions, as well as
141 their associated input and output variables, are detailed in sections 2.3.2 and 2.3.3.

142 **2.2.2 The sediment core simulation (*seamus_run*)**

143 The *seamus_run* module uses the required and optional input parameters specified by the user
144 (Table S1) to synthesise n number of single specimens being net-added to the historical layer of the
145 sediment core per simulation timestep, whereby n is scaled to the capacity of the synthetic sediment
146 archive being simulated (input variable *fpcm*) and to the SAR of the timestep as predicted by an
147 inputted age-depth relationship. The simulation creates large single specimen arrays of matching
148 dimensions for age (corresponding to the timestep), ‘unbioturbated’ sediment depth (according to
149 the age-depth input), as well as a ^{14}C age (in ^{14}C yrs) and ^{14}C activity (in *fMC*). The user also has the
150 option to input a ^{14}C blank value. Furthermore, all single specimens can be assigned carrier signal
151 values. It should be noted that the user is not required to enter input values for every timestep: for
152 example, an age-depth relationship can simply be inputted with a handful of data points and the
153 model will automatically linearly interpolate to create age and depth values for every simulation
154 timestep. The same principle holds true for other temporally dynamic inputs such as species
155 abundance, reservoir age and carrier signals.

156 After the creation of all new single specimens within the synthetic core, a per timestep bioturbation
157 simulation of the depth array is carried out. Specifically, for each timestep the depth values
158 corresponding to all simulated specimens within the timestep-specific active BD are each assigned a
159 new depth by way of uniform random sampling of the BD interval. In this way, uniform mixing of
160 specimens within the BD is simulated following established understanding of bioturbation. The per



161 timestep bioturbation simulation is carried out in *seamus_run* as follows; first, the simulation finds
162 the indices for all specimen depth values present in the contemporaneous BD:

```
163 ind = find(depths >= addepths(s) & depths < addepths(s) + biodepths(s))
```

164 Where *addepths(s)* is the depth corresponding to the age for timestep *s*, i.e. *addepths(s)* is
165 analogous to the timestep's core top; and where *biodepths(s)* is the BD corresponding to the age for
166 timestep *s*.

167 Subsequently, all specimen depth values corresponding to the active BD are assigned new depth
168 values by uniform random sampling of the active BD itself:

```
169 depths(ind) = rand(length(ind),1)*biodepths(s) + addepths(s)
```

170 The simulation uses a simple counter array to keep track of how many times each single specimen
171 has been subjected to a bioturbation cycle:

```
172 cycles(ind) = cycles(ind) + 1
```

173 All of the aforementioned processes are repeated for every simulation timestep until such point that
174 the end of the age-depth input (i.e. the final core top) is reached. Currently, the simulation carries
175 out bioturbation according to a per timestep uniform random sampling, but users wishing to
176 experiment with other types of bioturbation (i.e. partial bioturbation, etc.) can modify the
177 aforementioned lines of the script.

178 It is recommended that users initiate the *seamus_run* simulation with sufficient spinup time. The
179 necessary spin-up time can vary dependent upon the SAR and BD being studied, but for most
180 applications (SAR >5 cm/ka), a spin-up time of at least 20 ka should suffice. In other words, if one is
181 studying a period of interest that commences at 50 ka ago, then the simulation can be started at 70
182 ka ago. The required input parameters should be inputted in the command line as follows:

```
183 seamus_run(simstart, siminc, simend, btinc, fpcm, realD14C, blankbg,  
184 adpoints, bdpoints, savename)
```

185 Optional parameters can be additionally specified as follows, e.g. in the case of including the matrix
186 *matrixname* containing temporal changes in reservoir age for Species A:

```
187 seamus_run(simstart, siminc, simend, btinc, fpcm, realD14C, blankbg,  
188 adpoints, bdpoints, savename, 'resageA', matrixname)
```

189 The *seamus_run* module outputs a .mat file containing a number of very large 1 arrays of the same
190 dimension, whereby each position in each array corresponds to the same simulated single



191 specimens. Output variables are detailed in Table S2. To improve performance and ease of use, all
192 output variables are simulated for all single specimens. For example, carrier signals specific to
193 Species A (carrierA) are simulated for both Species A and Species B. As all output variables are of the
194 same dimension, one can easily isolate the carrierA signals specific to the specimens of Species A
195 (*types* value of 0) using logical indexing:

```
196 carrierA(types == 0 , :)
```

197 and from a specific core depth interval (e.g. between 16 and 17 cm):

```
198 carrierA(types == 0 & depths >= 16 & depths < 17 , :)
```

199 **2.2.3 Virtual picking of the simulated sediment core (*seamus_pick*)**

200 The *seamus_pick* module carries out a simple picking simulation upon the simulated core generated
201 by *seamus_run*. Users are able to set a specific sample size (i.e. the number of single specimens to
202 be randomly picked per sample), sample picking interval (i.e. core slice thickness) and optionally
203 include information about the amount of broken/non-whole specimens. The latter parameter is set
204 as a fraction of the entire specimen population, whereby the fraction of the population that has
205 been through the most bioturbation cycles is assumed to be broken. For example, if the user sets the
206 fraction of broken specimens to 0.25, then the simulation will only randomly pick from the specimen
207 population with bioturbation cycles between the 1st and 75th percentiles. In this way, the preference
208 of a palaeoceanographer to pick whole specimens is simulated.

209 Within *seamus_pick*, virtual ¹⁴C laboratory analysis is carried out on the picked subsamples by
210 calculating the mean ¹⁴C activity (in fMC), after which the resulting mean fMC value is converted into
211 ¹⁴C age (in ¹⁴C yr). A realistic measurement error is also assigned to each ¹⁴C age, whereby a late
212 Holocene ¹⁴C age is assumed to have a measurement error of ±30 ¹⁴C yr, and a ¹⁴C age of just above
213 the blank value is assumed to have an error of ±200 ¹⁴C yr. Measurement errors for ages in between
214 are linearly scaled to ¹⁴C activity. Using the *MatCal* (Lougheed and Obrochta, 2016) calibration
215 software, ¹⁴C ages and errors are calibrated inline, after the application of a user-prescribed
216 calibration curve and downcore reservoir age.

217 The *seamus_pick* function is called from the command line:

```
218 seamus_pick(matfilein, matfileout, calcurve, pickint, Apickfordate,  
219 Bpickfordate)
```

220 Optional parameters can be additionally specified as follows, e.g. in the case of including the matrix
221 *matrixname* containing downcore changes in the fraction of broken specimens in Species A:



```
222 seamus_pick(matfilein, matfileout, calcurve, pickint, Apickfordate,  
223 Bpickfordate, 'Abroken', matrixname)
```

224 **2.2.4 Suggested input data**

225 Users are free to use any input data they please, so long as it abides to the specified requirements as
226 listed in the function documentation, as well as in Tables S1 and S3. This freedom can allow users to
227 carry out abstract modelling experiments to increase understanding of the relationship between
228 input variables, the resulting downcore single specimen vales and trends in downcore discrete-depth
229 means. Alternatively, users can try to forward model an actual sediment core record in order to
230 investigate for the possible presence of bioturbation/abundance artefacts within their sediment core
231 record. An existing age-depth model of a sediment core could be used as the dynamic age-depth
232 input for the SEAMUS simulation, although users must be aware that age-depth models may
233 themselves contain artefacts caused by the interaction between bioturbation and abundance. Data
234 regarding downcore abundance estimates could be used as abundance estimates, but similarly,
235 users should be aware that observed downcore abundance in the core depth domain is not the same
236 as original abundance in the time domain. Users could, therefore, experiment in using multiple
237 temporal abundance and bioturbation depth combinations as simulation input, and rerunning the
238 simulation with different temporal abundance and bioturbation depth combinations until such time
239 that generated abundance data in depth is similar to the observed abundance in depth. Input
240 climate data for simulations could be based on multiple experimental, fictional scenarios, geological
241 records, or generated from isotope-enabled climate models (Roche, 2013) coupled to, for example, a
242 foraminifera ecology model such as FORAMCLIM (Lombard et al., 2011) or FAME (Roche et al., 2018;
243 Metcalfe et al., 2019a), to produce a fully parameterised “climate to sediment core” model
244 workflow.

245 **3.0 Model Evaluation**

246 **3.1 Comparison with TURBO2**

247 In order to evaluate the performance of the SEAMUS model, it is compared here to the output of the
248 established TURBO2 bioturbation model (Trauth, 2013), which was also authored in Matlab. The
249 most notable difference between SEAMUS and TURBO2 is that the latter outputs data in the form of
250 the perturbation of the mean downcore signal, whereas SEAMUS takes advantage of recent
251 increases in available computer memory to store and output a very large array of single elements
252 (foraminifera specimens). The two models can be compared, therefore, by comparing the mean
253 downcore output from TURBO2 with the SEAMUS downcore mean value derived from discrete-



254 depth single specimen populations. To achieve this comparison, the NGRIP Greenland ice core $\delta^{18}\text{O}$
255 record on the GICC05 timescale (North Greenland Ice Core Project members, 2004; Rasmussen et al.,
256 2014; Seierstad et al., 2014) is used as a reference signal to represent the ‘unbioturbated’ climate
257 signal (Fig. 1a). This 50 year temporal resolution signal is subsequently inputted into both SEAMUS
258 and TURBO2 using identical run conditions comprising of a constant SAR of 10 cm/ka, a constant BD
259 of 10 cm and a single foraminiferal species with a constant abundance. The SEAMUS simulation is
260 run using a 10 year timestep. The TURBO2 and SEAMUS core simulations (i.e. single specimens in the
261 case of SEAMUS) are directly assigned the oxygen isotope values from the NGRIP record. One would
262 obviously not expect that foraminifera in the open ocean would have the same oxygen isotope
263 values as an ice sheet record (due to fractionation effects, habitat effects, oceanographic effects,
264 seasonal overprint, etc), but the purpose here is simply to compare the output of the respective
265 bioturbation algorithms in SEAMUS and TURBO2 using some kind of high-temporal resolution
266 climatic input signal. Furthermore, using the NGRIP record allows for the isolation of the
267 bioturbation effect upon a hypothesised single specimen record. The respective mean downcore
268 bioturbated signals produced by SEAMUS and TURBO2 are shown in Fig. 1b and exhibit a significant
269 correlation ($r^2 = 0.99$, $p < 0.01$), indicating that the SEAMUS approach is incorporating the same
270 understanding of bioturbation as TURBO2.

271 **3.2 Processing speed and computing requirements**

272 Where possible, the processing of variables for simulation timesteps has been vectorised (i.e. not
273 processed within an iterative loop), in order to maximise processing speed. For example, the per
274 timestep assignment of single specimen arrays corresponding to ages and carrier signals all occurs
275 within fully vectorised code. However, the bioturbation simulation (i.e. the bioturbation of the
276 assigned depth values) is not vectorised and is carried out within a single-thread iterative loop, due
277 to each iteration of the bioturbation simulation being dependent upon the results of the previous
278 iteration. In order to optimise the processing time on 64-bit computers, all arrays are stored as 64-
279 bit. Should the user wish to save memory, it is possible to select the *do32bit* option when accessing
280 *seamus_run* from the command line (see Table S1). Indicative run times and memory use are shown
281 in Table 1.

282 The SEAMUS model was developed in Matlab 2017b. The *seamus_run* module can be run using the
283 basic Matlab environment, with no extra toolboxes. The *seamus_pick* module runs more efficiently
284 when the Statistics and Machine Learning toolbox (specifically, the *prctile* function) is installed, but
285 when it is detected that users do not have access to that toolbox, *seamus_pick* will revert to using a
286 modified version of the equivalent function in Octave (Kienzle, 2001), which has been embedded



287 into the script. The *seamus_pick* function also requires the Matcal (Lougheed and Obrochta, 2016)
288 ¹⁴C calibration script, which has been included in the SEAMUS download package.

289 **4.0 Potential model applications**

290 **4.1 Analysing downcore specimen population distributions**

291 As outlined in the introduction, advances in mass spectrometry have allowed for routine single
292 specimen analysis, which has led to increased interest in using analysis of single specimen
293 populations from discrete depths as a potentially powerful tool with which to reconstruct past
294 changes in climate variability. This application of this tool, however, still relies upon median
295 downcore age by assigning an age estimate to all single specimens from a single depth. Climate
296 variability/seasonality interpretations are clouded, therefore, when single specimens from a wide
297 range of ages are mixed into the same depth, especially if the interpretation relies upon detecting
298 extreme climate events in the form of single specimen outliers. Using the previously described
299 (Section 3.1; Fig 1b) SEAMUS simulation, it is possible to construct a probability heatmap and 95.45%
300 intervals for the single specimen $\delta^{18}\text{O}$ (Fig. 2a) data. The shape and range of these 95.45% intervals
301 relative to a glacial-interglacial change is similar to what has been previously calculated by
302 (Schiffelbein, 1986), albeit in the case of the Termination II deglaciation. Using SEAMUS, histograms
303 of single specimen $\delta^{18}\text{O}$ values for discrete depths can also be explored, for example for sediment
304 core intervals with a median downcore age corresponding to the early Holocene (Fig. 2b), mid-
305 Holocene (Fig. 2c), Younger Dryas (Fig. 2d) and Late Glacial Maximum (Fig. 2e). This analysis
306 demonstrates the potential for the presence of single specimens with glacial climate values being
307 present in samples with an interglacial mean value. For example, in the early Holocene depth
308 interval (Fig. 2c), 15% of the simulated single specimens have a $\delta^{18}\text{O}$ value less than or equal to -
309 36‰. Of course, some sediment archives may have much higher lower SAR than the constant 10
310 cm/ka simulated in this example. The contribution of older specimens to a particular depth interval
311 is dependent upon a number of factors; temporal changes in SAR, BD, species abundance and the
312 susceptibility of older specimens to be broken/dissolved as a consequence of having been through
313 more bioturbation cycles (Rubin and Suess, 1955; Ericson et al., 1956; Emiliani and Milliman, 1966;
314 Barker et al., 2007). Using the SEAMUS model it is possible to run dynamic sediment scenarios to
315 investigate the influence of mixing of specimens of different ages upon interpretations based upon
316 single specimen analysis.

317



318 4.2 Analysing ^{14}C calibration skill

319 As outlined earlier, it is possible to assign ^{14}C activities to single specimens in the sedimentation
320 simulation based by using suitable records of the Earth's $\Delta^{14}\text{C}$ history (e.g., *IntCal*). Subsequently,
321 SEAMUS uses the ^{14}C activities of the specimens contained within each discrete depth to calculate
322 and expected laboratory ^{14}C determination and measurement uncertainty. Using the *MatCal*
323 software, it is subsequently possible to calibrate the aforementioned ^{14}C age, in combination with a
324 calibration curve and reservoir age estimate, to produce an expected calibrated age distribution. The
325 calibrated age distribution for the discrete depth can be compared with the true age distribution for
326 the discrete depth, as recorded by the simulation, to evaluate the skill with which current ^{14}C dating
327 and calibration processes can reproduce the true age distribution of a particular sediment core slice.
328 A graphical representation of the aforementioned output for a discrete depth interval is shown in
329 Fig. 3, once again using the SEAMUS bioturbation simulation detailed in Section 3.1. This analysis
330 demonstrates that, for the applied simulation parameters and for the discrete depth interval
331 analysed in Fig. 3 (121-122 cm), the ^{14}C calibration process would produce a median calibrated age
332 of 12.21 cal ka BP, whereas the true median age is 11.79 ka, meaning that there is a 420 year
333 difference between the two. Furthermore, the ^{14}C calibration process produces a 95.45% credible
334 interval of 12.64 – 11.65 cal ka BP (a range of 990 cal yr), whereas the true 95.45% interval of the
335 single specimens within the simulation is 14.95-11.16 ka (a range of 3788 years), meaning that the
336 ^{14}C dating and calibration process considerably underestimates (by some 2800 years) the age
337 uncertainty for this particular interval of simulated sediment core. A Matlab script enabling users to
338 produce a figure similar to Fig. 3 is included within the tutorial script (*tutorial.m*) that is bundled with
339 SEAMUS. Users can subsequently explore downcore changes in the effectiveness of ^{14}C dating to
340 accurately estimate true age under various dynamic simulation conditions, including: abundance
341 changes, SAR changes, bioturbation depth changes, reservoir age changes, as well as during periods
342 of dynamic $\Delta^{14}\text{C}$.

343 4.3 Investigating noise created by the picking process

344 When picking discrete-depth samples from discrete-depth specimen populations,
345 palaeoceanographers randomly pick whole specimens to produce a downcore mean signal. The
346 *seamus_pick* module can be used to test for random noise introduced upon the mean signal by the
347 picking process. The module can be repeatedly run with a set number of randomly picked whole
348 specimens per sample, and the resulting picking runs can be compared to an ideal picking run that
349 picks all available whole specimens for each discrete depth. Such an approach is investigated here,
350 once again using the same SEAMUS bioturbation simulation that was carried out in Section 3.1, for



351 picking scenarios each with one specimen per sample (Fig. 4a), two specimens per sample (Fig. 4b),
352 three specimens per sample (Fig. 4c), five specimens per sample (Fig. 4d), 10 specimens per sample
353 (Fig. 4e) and 20 specimens per sample (Fig. 4f). Such simulations can allow researchers to isolate and
354 quantify the effect of the picking process upon their downcore multi-specimen reconstructions for
355 their particular sediment core scenario. It can be noted that for the 10 cm/ka simulation carried out
356 here, that large sample sizes ($n \geq 10$) tend to produce downcore sampling runs close to the total
357 population mean (Figs. 4E and 4F), although the true spread of values is hidden. Furthermore, even
358 with larger samples sizes there is still the possibility for the generation of picking noise-induced
359 peak/trough values which could be erroneously interpreted as a precise indication of the timing of a
360 particular climate feature. In the case of very small sample sizes (Figs. 4A and 4B), researchers can
361 get an idea of the total spread of values within single core intervals. With advances in mass
362 spectrometry making the analysis of single specimens ever more routine and cost-effective, the ideal
363 approach in the future may involve exclusively analysing single specimens, with single specimen
364 values from discrete depths used to both estimate the signal distribution and calculate a downcore
365 mean signal, thus facilitating a 'best of both worlds' approach.

366 4.4 Investigating noise created by absolute specimen abundance

367 The interaction between total specimen abundance and bioturbation creates downcore noise in the
368 sedimentary record. In Fig. 5, the downcore, discrete-depth median age increase per centimetre for
369 three SEAMUS simulations all with an idealised constant SAR of 10 cm ka⁻¹ and constant BD of 10 cm
370 is shown, with the number of outputted specimens per centimetre being set differently for each
371 simulation, namely at 10² specimens per cm (Fig. 5a), 10³ specimens per cm (Fig. 5b) and 10⁴
372 specimens per cm (Fig. 5c). In all three scenarios the downcore, discrete-depth increase in median
373 age clusters around 100 years cm⁻¹, which is what would be expected in the case of 10 cm ka⁻¹
374 sediment core. As expected, the signal-to-noise ratio is higher in cases of higher abundance. An
375 interesting side-effect of a decreased signal-noise-ratio is the increased likelihood of the generation
376 of apparent age-depth reversals. For example, in the abundance scenario with 10² specimens cm⁻¹
377 (Fig. 5a), 21.7% of the discrete-depth (1 cm) age-depth points produce an apparent age-depth
378 reversal. Due to the fact that many age-depth modelling software packages often consider such age-
379 depth reversals as outliers (Blaauw and Christen, 2011; Lougheed and Obrochta, 2019),
380 palaeoceanographers should be aware that the apparent age-depth reversals generated by very
381 noisy downcore signals caused by low specimen abundance may result in age-depth models that are
382 biased towards young ages. Also, while palaeoceanographers often quantify relative abundance as a
383 ratio between different species, it is additionally important to quantify the absolute abundance of a



384 particular species being studied in the form of number of specimens per specific sediment volume,
385 as this can give clues regarding the expected signal to noise ratio ascertained from a discrete-depth
386 analysis.

387 **4.5 Investigating artefacts created by dynamic specimen abundance**

388 In the previous sections, scenarios involving constant specimen abundance were explored. SEAMUS
389 is specifically designed with the ability to process multiple temporally dynamic inputs. In Fig. 6, the
390 effect of temporally dynamic species abundance for a theorised “Species A” is studied, once again
391 using a scenario with a constant SAR of 10 cm/ka and constant BD of 10 cm. Past studies using
392 simpler mixing models have previously shown that the downcore $\delta^{18}\text{O}$ signal for particular species
393 can display offsets that are in fact an artefact of the interplay between abundance and bioturbation
394 (LÖwemark and Grootes, 2004; Trauth, 2013). Here, the single-specimen SEAMUS simulation is used
395 to investigate the effects of abundance and bioturbation upon the age-depth signal produced by
396 single specimens. In this scenario SEAMUS is driven using a dynamic input with six temporal maxima
397 in Species A specimen flux centred upon 10, 16 18, 28, 32 and 36 ka ago (Fig. 6a). The resulting post-
398 simulation absolute abundance of Species A in the depth domain (Fig. 6b) a smoothed out / mixing
399 of the abundance peaks as a result of bioturbation. The interaction between dynamic abundance
400 and bioturbation also has consequences for the discrete-depth age-depth relationship of Species A.
401 For example, the downcore change in discrete-depth median age for Species A (Fig. 6c) is less noisy
402 (i.e. less likely to produce outliers) for intervals close to the absolute abundance peaks, but
403 negatively offset from the target discrete-depth median age change of 100 years per cm that would
404 be associated with the 10 cm/ka sediment core simulation. This would be manifested in an age-
405 depth reconstruction as an age-depth plateau near to an abundance peak.

406 Similarly, the 95.45% discrete-depth age range for Species A is much more constrained in the case of
407 depth intervals located close to the abundance peaks (Fig. 6d), but less representative of the median
408 age for the total sediment (all specimens), with Species A being biased towards too young ages (Fig.
409 6e). This bias is an interesting finding, seeing as it has long been assumed that pooled specimen
410 samples used for dating (e.g., ^{14}C dating) should be retrieved from abundance peaks (Keigwin and
411 Lehman, 1994; Waelbroeck et al., 2001; Galbraith et al., 2015). This assumption is largely based on
412 the fact that ^{14}C dates sampled from abundance peaks are younger than the immediately
413 surrounding sediment (Rafter et al., 2018). However, the SEAMUS simulation suggests that
414 abundance peaks can result in ages that are anomalously young when compared to the total
415 sediment (Fig. 6e).



416 **5.0 Conclusion**

417 Deep-sea sediment archives are subject to systematic bioturbation, which can complicate
418 palaeoclimate reconstructions sourced from sediment cores. Complications can include artefacts
419 and/or spurious offsets in ^{14}C age other carrier signals (such as $\delta^{18}\text{O}$) sourced from multi-specimen
420 samples. The SEAMUS model allows users to interactively investigate how such artefacts and/or
421 spurious offsets can be attributed to the mixing of single specimens. The model is suitable for users
422 who are investigating the downcore mean signal and how it is affected by dynamic changes in input
423 variables. The model is especially interesting for researchers who are using single-specimen
424 foraminifera analysis to quantify past changes in seasonality or multi-centennial amplitude in
425 regional climate variability, as it can assist researchers in understanding the influence of bioturbation
426 upon their results and the interpretation. The model is also useful as a teaching resource; for
427 example, users can keep all but one input variable constant, and learn to understand the influence
428 of dynamic changes in that particular input variable upon the downcore specimen record.
429 Subsequently, multiple dynamic variables can be introduced.

430 **Code availability**

431 The SEAMUS model and accompanying interactive tutorial can be downloaded from the Zenodo
432 public repository: <https://doi.org/10.5281/zenodo.3251655>

433 **Acknowledgements**

434 This work was funded by Swedish Research Council (*Vetenskapsrådet* – VR) Starting Grant number
435 2018-04992. Thanks to LOG for hosting me as a guest researcher in Wimereux. Brett Metcalfe is
436 thanked for various discussions about the state-of-the-art of single specimen foraminifera analysis
437 (see also the resources at www.brett-metcalfe.com).

438 **References**

- 439 Bard, E., Arnold, M., Duprat, J., Moyes, J. and Duplessy, J. C.: Reconstruction of the last deglaciation:
440 Deconvolved records of $\delta^{18}\text{O}$ profiles, micropaleontological variations and accelerator mass
441 spectrometric ^{14}C dating, *Climate Dynamics*, 1(2), 101–112, 1987.
- 442 Barker, S., Broecker, W., Clark, E. and Hajdas, I.: Radiocarbon age offsets of foraminifera resulting
443 from differential dissolution and fragmentation within the sedimentary bioturbated zone,
444 *Paleoceanography*, 22(2), doi:10.1029/2006PA001354, 2007.
- 445 Berger, W. H. and Heath, G. R.: Vertical mixing in pelagic sediments, *Journal of Marine Research*, 26,
446 134–143, 1968.
- 447 Berger, W. H. and Johnson, R. F.: On the thickness and the ^{14}C age of the mixed layer in deep-sea
448 carbonates, *Earth and Planetary Science Letters*, 41(2), 223–227, 1978.



- 449 Berger, W. H. and Killingley, J. S.: Box cores from the equatorial Pacific: 14C sedimentation rates and
450 benthic mixing, *Marine Geology*, 45(1), 93–125, doi:10.1016/0025-3227(82)90182-7, 1982.
- 451 Billups, K. and Spero, H. J.: Reconstructing the stable isotope geochemistry and paleotemperatures
452 of the equatorial Atlantic during the last 150,000 years: Results from individual foraminifera,
453 *Paleoceanography*, 11(2), 217–238, doi:10.1029/95PA03773, 1996.
- 454 Blaauw, M. and Christen, J. A.: Flexible Paleoclimate Age-Depth Models Using an Autoregressive
455 Gamma Process, *Bayesian Analysis*, 6, 457–474, doi:10.1214/11-BA618, 2011.
- 456 Boudreau, B. P.: Mean mixed depth of sediments: The wherefore and the why, *Limnology and
457 Oceanography*, 43(3), 524–526, doi:10.4319/lo.1998.43.3.0524, 1998.
- 458 Dolman, A. M. and Laepple, T.: Sedproxy: a forward model for sediment archived climate proxies,
459 *Climate of the Past Discussions*, 1–31, doi:10.5194/cp-2018-13, 2018.
- 460 Emiliani, C. and Milliman, J. D.: Deep-sea sediments and their geological record, *Earth-Science
461 Reviews*, 1(2–3), 105–132, doi:10.1016/0012-8252(66)90002-X, 1966.
- 462 Ericson, D. B., Broecker, W. S., Kulp, J. L. and Wollin, G.: Late-Pleistocene Climates and Deep-Sea
463 Sediments, *Science*, 124(3218), 385–389, doi:10.1126/science.124.3218.385, 1956.
- 464 Ford, H. L. and Ravelo, A. C.: Estimates of Pliocene Tropical Pacific Temperature Sensitivity to
465 Radiative Greenhouse Gas Forcing, *Paleoceanography and Paleoclimatology*, 34(1), 2–15,
466 doi:10.1029/2018PA003461, 2019.
- 467 Ford, H. L., Ravelo, A. C. and Polissar, P. J.: Reduced El Nino-Southern Oscillation during the Last
468 Glacial Maximum, *Science*, 347(6219), 255–258, doi:10.1126/science.1258437, 2015.
- 469 Fraass, A. J. and Lowery, C. M.: Defining uncertainty and error in planktic foraminiferal oxygen
470 isotope measurements: Uncertainty in Foraminiferal Oxygen Isotopes, *Paleoceanography*, 32(2), 104–122,
471 doi:10.1002/2016PA003035, 2017.
- 472 Galbraith, E. D., Kwon, E. Y., Bianchi, D., Hain, M. P. and Sarmiento, J. L.: The impact of atmospheric
473 CO₂ on carbon isotope ratios of the atmosphere and ocean, *Global Biogeochemical Cycles*, 29(3),
474 307–324, doi:10.1002/2014GB004929, 2015.
- 475 Ganssen, G. M., Peeters, F. J. C., Metcalfe, B., Anand, P., Jung, S. J. A., Kroon, D. and Brummer, G.-J.
476 A.: Quantifying sea surface temperature ranges of the Arabian Sea for the past 20 000 years, *Climate
477 of the Past*, 7(4), 1337–1349, doi:10.5194/cp-7-1337-2011, 2011.
- 478 Keigwin, L. D. and Lehman, S. J.: Deep circulation change linked to HEINRICH Event 1 and Younger
479 Dryas in a middepth North Atlantic Core, *Paleoceanography*, 9(2), 185–194, doi:10.1029/94PA00032,
480 1994.
- 481 Kienzle, P.: Octave prctile() function., [online] Available from:
482 <https://sourceforge.net/p/octave/statistics/ci/c1ef33a337b30168a0581d9cae26397d2c1ae06a/tree/inst/prctile.m#l28>, 2001.
483
- 484 Killingley, J. S., Johnson, R. F. and Berger, W. H.: Oxygen and carbon isotopes of individual shells of
485 planktonic foraminifera from Ontong-Java plateau, equatorial pacific, , 12, 1981.



- 486 Lombard, F., Labeyrie, L., Michel, E., Bopp, L., Cortijo, E., Retailleau, S., Howa, H. and Jorissen, F.:
487 Modelling planktic foraminifer growth and distribution using an ecophysiological multi-species
488 approach, *Biogeosciences*, 8(4), 853–873, doi:10.5194/bg-8-853-2011, 2011.
- 489 Lougheed, B. C. and Obrochta, S. P.: MatCal: Open Source Bayesian 14C Age Calibration in Matlab,
490 *Journal of Open Research Software*, 4, doi:10.5334/jors.130, 2016.
- 491 Lougheed, B. C. and Obrochta, S. P.: A rapid, deterministic age-depth modelling routine for
492 geological sequences with inherent depth uncertainty, *Paleoceanography and Paleoclimatology*, 34,
493 122–133, doi:10.1029/2018PA003457, 2019.
- 494 Lougheed, B. C., Metcalfe, B., Ninnemann, U. S. and Wacker, L.: Moving beyond the age-depth model
495 paradigm in deep sea palaeoclimate archives: dual radiocarbon and stable isotope analysis on single
496 foraminifera, *Climate of the Past*, 14, 515–526, doi:10.5194/cp-2017-119, 2018.
- 497 Löwemark, L. and Grootes, P. M.: Large age differences between planktic foraminifers caused by
498 abundance variations and Zoophycos bioturbation., *Paleoceanography*, 19(2), PA2001,
499 doi:10.1029/2003PA000949, 2004.
- 500 Metcalfe, B., Feldmeijer, W., de Vringer-Picon, M., Brummer, G.-J. A., Peeters, F. J. C. and Ganssen,
501 G. M.: Late Pleistocene glacial–interglacial shell-size–isotope variability in planktonic foraminifera as
502 a function of local hydrography, *Biogeosciences*, 12(15), 4781–4807, doi:10.5194/bg-12-4781-2015,
503 2015.
- 504 Metcalfe, B., Lougheed, B. C., Waelbroeck, C. and Roche, D. M.: On the validity of foraminifera-based
505 ENSO reconstructions, *Climate of the Past Discussions*, 1–31, doi:https://doi.org/10.5194/cp-2019-9,
506 2019a.
- 507 Metcalfe, B., Feldmeijer, W. and Ganssen, G. M.: Oxygen Isotope Variability of Planktonic
508 Foraminifera Provide Clues to Past Upper Ocean Seasonal Variability, *Paleoceanography and*
509 *Paleoclimatology*, 34(3), 374–393, doi:10.1029/2018PA003475, 2019b.
- 510 North Greenland Ice Core Project members: High-resolution record of Northern Hemisphere climate
511 extending into the last interglacial period, *Nature*, 431(7005), 147–151, doi:10.1038/nature02805,
512 2004.
- 513 Peng, T.-H., Broecker, W. S. and Berger, W. H.: Rates of benthic mixing in deep-sea sediment as
514 determined by radioactive tracers, *Quaternary Research*, 11(1), 141–149, 1979.
- 515 Pias, N. G.: Geologic time series from deep-sea sediments: Time scales and distortion by
516 bioturbation, *Marine Geology*, 51(1–2), 99–113, 1983.
- 517 Rafter, P. A., Herguera, J.-C. and Southon, J. R.: Extreme lowering of deglacial seawater radiocarbon
518 recorded by both epifaunal and infaunal benthic foraminifera in a wood-dated sediment core, *Clim.*
519 *Past*, 14(12), 1977–1989, doi:10.5194/cp-14-1977-2018, 2018.
- 520 Rasmussen, S. O., Bigler, M., Blockley, S. P., Blunier, T., Buchardt, S. L., Clausen, H. B., Cvijanovic, I.,
521 Dahl-Jensen, D., Johnsen, S. J., Fischer, H., Gkinis, V., Guillevic, M., Hoek, W. Z., Lowe, J. J., Pedro, J.
522 B., Popp, T., Seierstad, I. K., Steffensen, J. P., Svensson, A. M., Vallelonga, P., Vinther, B. M., Walker,
523 M. J. C., Wheatley, J. J. and Winstrup, M.: A stratigraphic framework for abrupt climatic changes
524 during the Last Glacial period based on three synchronized Greenland ice-core records: refining and
525 extending the INTIMATE event stratigraphy, *Quaternary Science Reviews*, 106, 14–28,
526 doi:10.1016/j.quascirev.2014.09.007, 2014.



- 527 Reimer, P. J., Bard, E., Bayliss, A., Beck, J. W., Blackwell, P. G., Ramsey, C. B., Buck, C. E., Cheng, H.,
528 Edwards, R. L., Friedrich, M., Grootes, P. M., Guilderson, T. P., Haflidason, H., Hajdas, I., Hatté, C.,
529 Heaton, T. J., Hoffmann, D. L., Hogg, A. G., Hughen, K. A., Kaiser, K. F., Kromer, B., Manning, S. W.,
530 Niu, M., Reimer, R. W., Richards, D. A., Scott, E. M., Southon, J. R., Staff, R. A., Turney, C. S. M. and
531 van der Plicht, J.: IntCal13 and Marine13 Radiocarbon Age Calibration Curves 0–50,000 Years cal BP,
532 Radiocarbon, 55(04), 1869–1887, 2013.
- 533 Roche, D. M.: $\delta^{18}\text{O}$ water isotope in the iLOVECLIM model (version 1.0) – Part 1: Implementation
534 and verification, Geosci. Model Dev., 6(5), 1481–1491, doi:10.5194/gmd-6-1481-2013, 2013.
- 535 Roche, D. M., Waelbroeck, C., Metcalfe, B. and Caley, T.: FAME (v1.0): a simple module to simulate
536 the effect of planktonic foraminifer species-specific habitat on their oxygen isotopic content,
537 Geoscientific Model Development, 11(9), 3587–3603, doi:10.5194/gmd-11-3587-2018, 2018.
- 538 Rubin, M. and Suess, H. E.: U.S. Geological Survey Radiocarbon Dates 11., Science, 121, 481–488,
539 1955.
- 540 Schifflbein, P.: Effect of benthic mixing on the information content of deep-sea stratigraphical
541 signals, Nature, 311(5987), 651, doi:10.1038/311651a0, 1984.
- 542 Schifflbein, P.: The interpretation of stable isotopes in deep-sea sediments: An error analysis case
543 study, Marine Geology, 70(3–4), 313–320, doi:10.1016/0025-3227(86)90008-3, 1986.
- 544 Seierstad, I. K., Abbott, P. M., Bigler, M., Blunier, T., Bourne, A. J., Brook, E., Buchardt, S. L., Buizert,
545 C., Clausen, H. B., Cook, E., Dahl-Jensen, D., Davies, S. M., Guillevic, M., Johnsen, S. J., Pedersen, D. S.,
546 Popp, T. J., Rasmussen, S. O., Severinghaus, J. P., Svensson, A. and Vinther, B. M.: Consistently dated
547 records from the Greenland GRIP, GISP2 and NGRIP ice cores for the past 104 ka reveal regional
548 millennial-scale $\delta^{18}\text{O}$ gradients with possible Heinrich event imprint, Quaternary Science Reviews,
549 106, 29–46, doi:10.1016/j.quascirev.2014.10.032, 2014.
- 550 Spero, H. J. and Williams, D. F.: Evidence for seasonal low-salinity surface waters in the Gulf of
551 Mexico over the last 16,000 years, Paleoceanography, 5(6), 963–975,
552 doi:10.1029/PA005i006p00963, 1990.
- 553 Tang, C. M. and Stott, L. D.: Seasonal salinity changes during Mediterranean sapropel deposition
554 9000 years B.P.: Evidence from isotopic analyses of individual planktonic foraminifera,
555 Paleoceanography, 8(4), 473–493, doi:10.1029/93PA01319, 1993.
- 556 Thirumalai, K., Partin, J. W., Jackson, C. S. and Quinn, T. M.: Statistical constraints on El Niño
557 Southern Oscillation reconstructions using individual foraminifera: A sensitivity analysis: IFA-ENSO
558 UNCERTAINTY, Paleoceanography, 28(3), 401–412, doi:10.1002/palo.20037, 2013.
- 559 Trauth, M. H.: TURBO: a dynamic-probabilistic simulation to study the effects of bioturbation on
560 paleoceanographic time series, Computers & Geosciences, 24(5), 433–441, doi:10.1016/S0098-
561 3004(98)00019-3, 1998.
- 562 Trauth, M. H.: TURBO2: A MATLAB simulation to study the effects of bioturbation on
563 paleoceanographic time series, Computers & Geosciences, 61, 1–10,
564 doi:10.1016/j.cageo.2013.05.003, 2013.
- 565 Trauth, M. H., Sarnthein, M. and Arnold, M.: Bioturbational mixing depth and carbon flux at the
566 seafloor, Paleoceanography, 12(3), 517–526, 1997.



- 567 Waelbroeck, C., Duplessy, J.-C., Michel, E., Labeyrie, L., Paillard, D. and Duprat, J.: The timing of the
568 last deglaciation in North Atlantic climate records, *Nature*, 412, 724–727, 2001.
- 569 Wit, J. C., Reichert, G. J. and Ganssen, G. M.: Unmixing of stable isotope signals using single specimen
570 $\delta^{18}\text{O}$ analyses, *Geochemistry, Geophysics, Geosystems*, 14(4), 1312–1320, doi:10.1002/ggge.20101,
571 2013.
- 572
- 573



574 Table 1. Approximate run times and Matlab memory use in the case of a 70 ka simulation run with
575 10 year iterations and core capacity of 10^2 , 10^3 and 10^4 specimens per cm. The runs carried out using
576 Matlab 2017b on a 64-bit system with 8GB of RAM and an Intel i7-2600 processor.

	10^2 specimens cm^{-1}	10^3 specimens cm^{-1}	10^4 specimens cm^{-1}
<i>seamus_run</i>	2.5 s / 0.62 GB	19.7 s / 0.66 GB	237.5 s / 1.15 GB
<i>seamus_pick</i>	11.4 s / 0.61 GB	13.2 s / 0.64 GB	37.8 s / 0.99 GB

577



578 **Figure captions (also included with figures)**

579 Figure 1. **(a)** NGRIP $\delta^{18}\text{O}$ record (North Greenland Ice Core Project members, 2004) plotted using the
580 latest GICC05 timescale (Rasmussen et al., 2014; Seierstad et al., 2014), adjusted by 50 years so that
581 1950 BCE is equivalent to 'present'. **(b)** Result of SEAMUS run using the NGRIP $\delta^{18}\text{O}$ data as temporal
582 input data. SEAMUS run settings are shown in the panel inset. Also shown is the average of ten runs
583 of TURBO2 (Trauth, 2013), based on the same NGRIP input data and using a SAR of 10 cm ka^{-1} and a
584 constant BD of 10 cm.

585 Figure 2. **(a)** Log heat map (in greyscale) of downcore single specimen $\delta^{18}\text{O}$ value probability in the
586 form of a 0.25% by 1 cm matrix, based on the single specimen data from the SEAMUS run displayed
587 in Fig 1B. The probability for each matrix element is calculated as the number of specimens for each
588 discrete depth within a given 0.25% range, divided by the total number of specimens contained
589 within the discrete depth. The natural logarithm of the probability is subsequently plotted, in order
590 to increase visibility of low probability areas in the heat map. Also shown (in orange) are the $\delta^{18}\text{O}$
591 values corresponding to the mean and 95.45% intervals for each discrete depth interval. **(b, c, d and**
592 **e)** Single specimen $\delta^{18}\text{O}$ histograms for various discrete-depth intervals.

593 Figure 3. Example of using output from a SEAMUS simulation to estimate ^{14}C calibration skill for a
594 particular discrete-depth subsample. The green histograms represent the SEAMUS simulation
595 output: on the x-axis the true age distribution of the discrete-depth single specimens (with the green
596 diamond corresponding to the median true age), and on the y-axis the ^{14}C age distribution of the
597 single specimens (with the green diamond corresponding to the mean ^{14}C age). All histograms are
598 shown using 100 (^{14}C) year bins. The orange probability distribution on the y-axis represents a
599 normal distribution corresponding to an idealised laboratory ^{14}C analysis of the single specimens,
600 where the orange square corresponds to the expected mean laboratory ^{14}C age. The orange
601 probability distribution on the x-axis represents the calibrated age distribution arising from the
602 calibration of the laboratory ^{14}C analysis using *Marine13* (Reimer et al., 2013). Also shown, for
603 reference, are the *Marine13* calibration curve 1sigma (dark grey) and 2sigma (light grey) confidence
604 intervals. Simulation output shown in the figure is based on the SEAMUS run in Fig 1B, with ^{14}C
605 activities assigned to single specimens according to *Marine13* with a constant ΔR of $0 \pm 0 \text{ }^{14}\text{C yr}$. For
606 the picking and calibration, all single specimens within the 121-122 cm discrete depth are picked,
607 and calibration is carried out using *MatCal* (Lougheed and Obrochta, 2016) with *Marine13* and a ΔR
608 of $0 \pm 0 \text{ }^{14}\text{C yr}$.



609 Figure 4. Estimating noise induced by subsample size during the picking process. Based on the
610 SEAMUS simulation in Fig. 1b, six sample size scenarios are considered: **(a)** one specimen per
611 sample; **(b)** two specimens per sample; **(c)** three specimens per sample; **(d)** five specimens per
612 sample; **(e)** ten specimens per sample; **(f)** 20 specimens per sample. In each scenario, the downcore
613 picking process is repeated 10 times, and each picking run is represented by a coloured line. Also
614 shown in all panels is the mean $\delta^{18}\text{O}$ value for all single specimens within discrete depth intervals
615 (black line) and 95.45% intervals (filled grey area).

616 Figure 5. Estimating downcore age-depth noise induced by absolute species abundance in three
617 scenarios all involving involving a constant SAR of 10 cm ka^{-1} and constant bioturbation depth of 10 cm .
618 In all three panels, the data points (circles) indicate the downcore discrete-depth median age
619 increase for each cm of core depth. Green circles correspond to positive downcore median age
620 change, while orange data points correspond to negative downcore median age change (i.e.
621 apparent age reversals). The horizontal black line in each panel denotes the perfect downcore age
622 change of $+100\text{ years cm}^{-1}$ that would be associated with a constant SAR of 10 cm ka^{-1} . The yellow
623 interval denotes the still-active BD (10 cm) at the core top. The signal-to-noise ratio (SNR) is also
624 computed for each scenario as the ratio between the summed squared magnitudes of the signal and
625 of the noise. The still-active BD at the core top is excluded from the SNR calculation. Three different
626 abundance scenarios are shown: **(a)** constant abundance of $10^2\text{ specimens cm}^{-1}$. **(b)** constant
627 abundance of $10^3\text{ specimens cm}^{-1}$. **(c)** constant abundance of $10^4\text{ specimens cm}^{-1}$.

628 Figure 6. Investigating the effect of temporal changes in a species' abundance upon its discrete-
629 depth age-depth signal in the case of a simulated sediment core with a constant SAR of 10 cm ka and
630 constant BD of 10 cm . In all panels, the yellow interval denotes the still-active BD (10 cm) at the core
631 top. **(a)** The temporal abundance for a given species "Species A" used in the SEAMUS simulation,
632 inputted into the model as a fraction of the per timestep specimen flux. **(b)** The resulting simulated
633 downcore, discrete-depth (1 cm) absolute abundance (number of specimens) for Species A. Vertical
634 grey bands correspond to the depth of the abundance peaks. **(c)** The downcore, discrete-depth (1 cm)
635 change in median age based on samples containing only Species A specimens. Green circles
636 denote downcore increase in discrete-depth apparent median age (i.e. positive apparent SAR) and
637 orange circles denote downcore decrease in discrete-depth median age (i.e. apparent age reversals).
638 The horizontal black line in each panel denotes the perfect downcore age change of $+100\text{ years cm}^{-1}$
639 that would be associated with a constant SAR of 10 cm ka^{-1} . **(d)** The 95.45% age range of for Species
640 A for each discrete 1 cm depth. **(e)** The offset between the median age of Species A (Med_A) and the



- 641 median age of all specimens (Med_{all}). Shown in the panel is $Med_A - Med_{all}$. The horizontal black line
642 represents corresponds to zero (i.e., no offset).

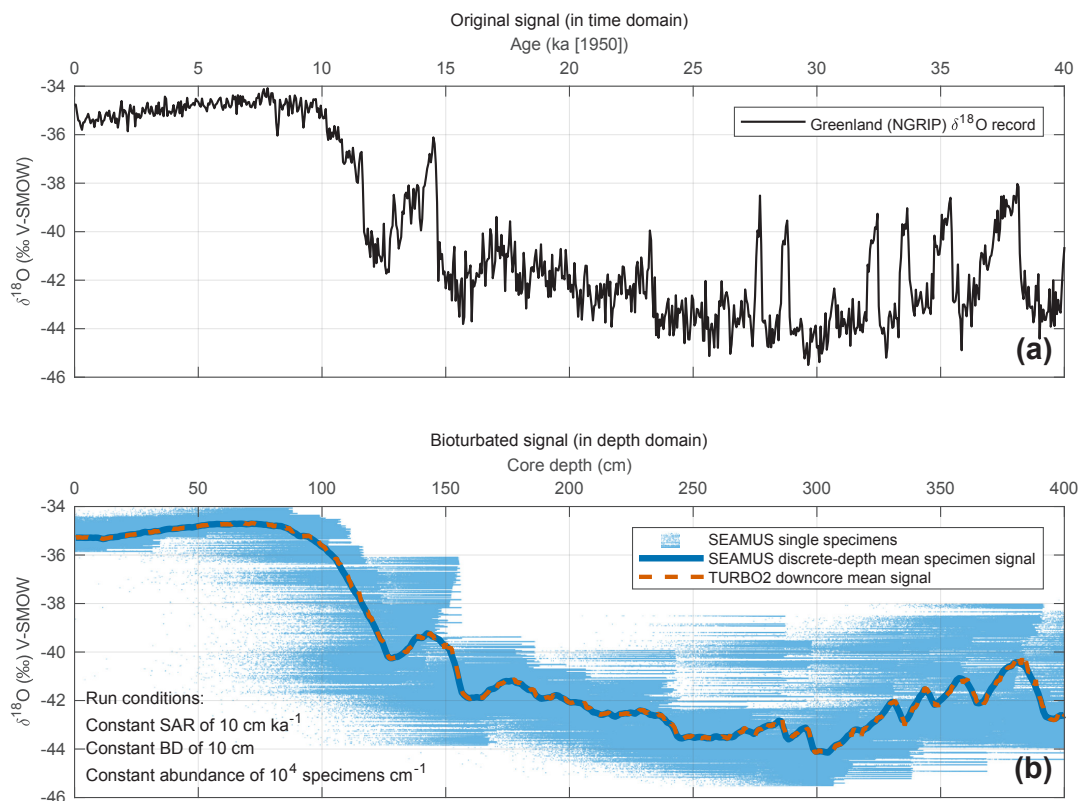


Figure 1. **(a)** NGRIP $\delta^{18}\text{O}$ record (North Greenland Ice Core Project members, 2004) plotted using the latest GICC05 timescale (Rasmussen et al., 2014; Seierstad et al., 2014), adjusted by 50 years so that 1950 BCE is equivalent to 'present'. **(b)** Result of SEAMUS run using the NGRIP $\delta^{18}\text{O}$ data as temporal input data. SEAMUS run settings are shown in the panel inset. Also shown is the average of ten runs of TURBO2 (Trauth, 2013), based on the same NGRIP input data and using a SAR of 10 cm ka^{-1} and a constant BD of 10 cm.

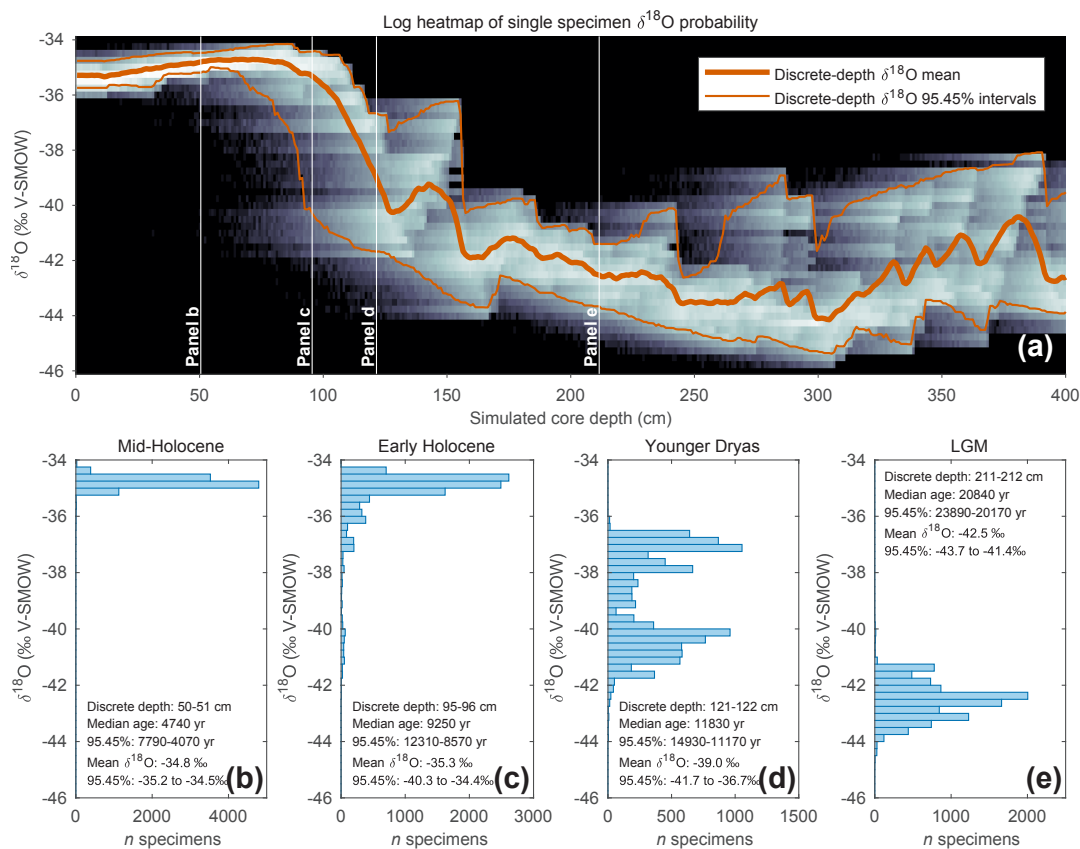


Figure 2. **(a)** Log heat map (in greyscale) of downcore single specimen $\delta^{18}\text{O}$ value probability in the form of a 0.25‰ by 1 cm matrix, based on the single specimen data from the SEAMUS run displayed in Fig 1B. The probability for each matrix element is calculated as the number of specimens for each discrete depth within a given 0.25‰ range, divided by the total number of specimens contained within the discrete depth. The natural logarithm of the probability is subsequently plotted, in order to increase visibility of low probability areas in the heat map. Also shown (in orange) are the $\delta^{18}\text{O}$ values corresponding to the mean and 95.45% intervals for each discrete depth interval. **(b, c, d and e)** Single specimen $\delta^{18}\text{O}$ histograms for various discrete-depth intervals.

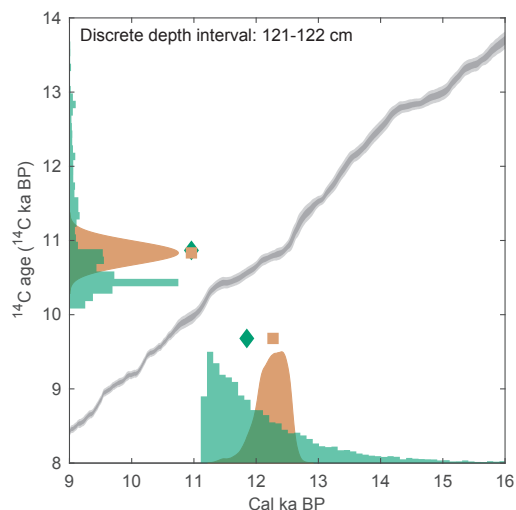


Figure 3. Example of using output from a SEAMUS simulation to estimate ^{14}C calibration skill for a particular discrete-depth subsample. The green histograms represent the SEAMUS simulation output: on the x-axis the true age distribution of the discrete-depth single specimens (with the green diamond corresponding to the median true age), and on the y-axis the ^{14}C age distribution of the single specimens (with the green diamond corresponding to the mean ^{14}C age). All histograms are shown using 100 (^{14}C) year bins. The orange probability distribution on the y-axis represents a normal distribution corresponding to an idealised laboratory ^{14}C analysis of the single specimens, where the orange square corresponds to the expected mean laboratory ^{14}C age. The orange probability distribution on the x-axis represents the calibrated age distribution arising from the calibration of the laboratory ^{14}C analysis using *Marine13* (Reimer et al., 2013). Also shown, for reference, are the *Marine13* calibration curve 1sigma (dark grey) and 2sigma (light grey) confidence intervals. Simulation output shown in the figure is based on the SEAMUS run in Fig 1B, with ^{14}C activities assigned to single specimens according to *Marine13* with a constant ΔR of 0 ± 0 ^{14}C yr. For the picking and calibration, all single specimens within the 121-122 cm discrete depth are picked, and calibration is carried out using *MatCal* (Lougheed and Obrochta, 2016) with *Marine13* and a ΔR of 0 ± 0 ^{14}C yr.

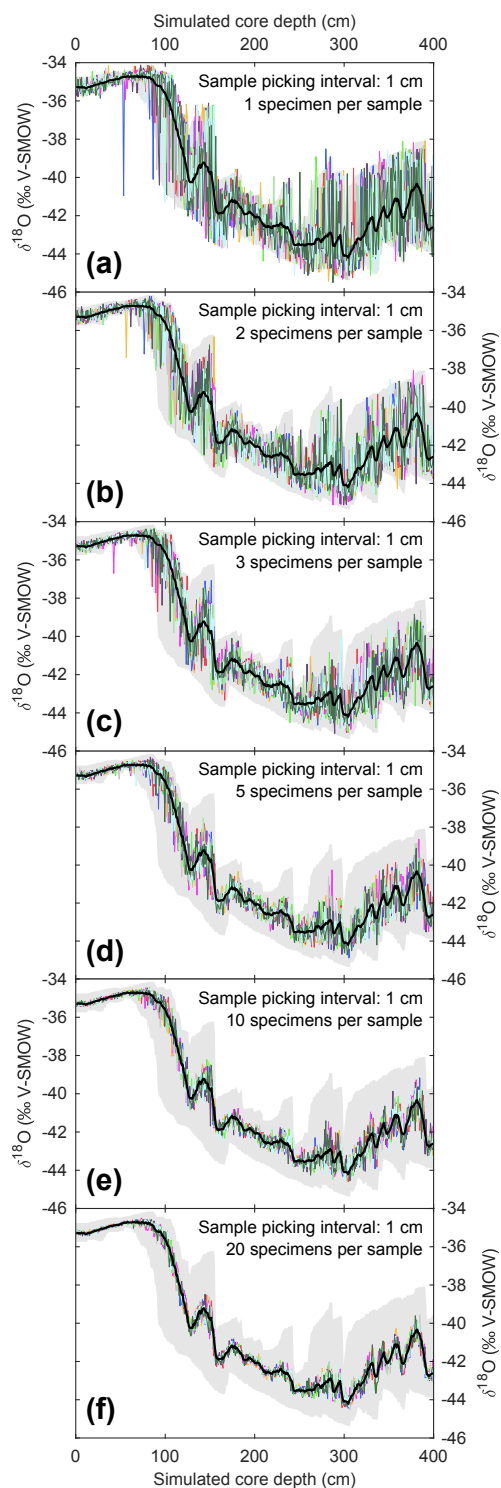


Figure 4. Estimating noise induced by subsample size during the picking process. Based on the SEAMUS simulation in Fig. 1b, six sample size scenarios are considered: **(a)** one specimen per sample; **(b)** two specimens per sample; **(c)** three specimens per sample; **(d)** five specimens per sample; **(e)** ten specimens per sample; **(f)** 20 specimens per sample. In each scenario, the downcore picking process is repeated 10 times, and each picking run is represented by a coloured line. Also shown in all panels is the mean $\delta^{18}\text{O}$ value for all single specimens within discrete depth intervals (black line) and 95.45% intervals (filled grey area).

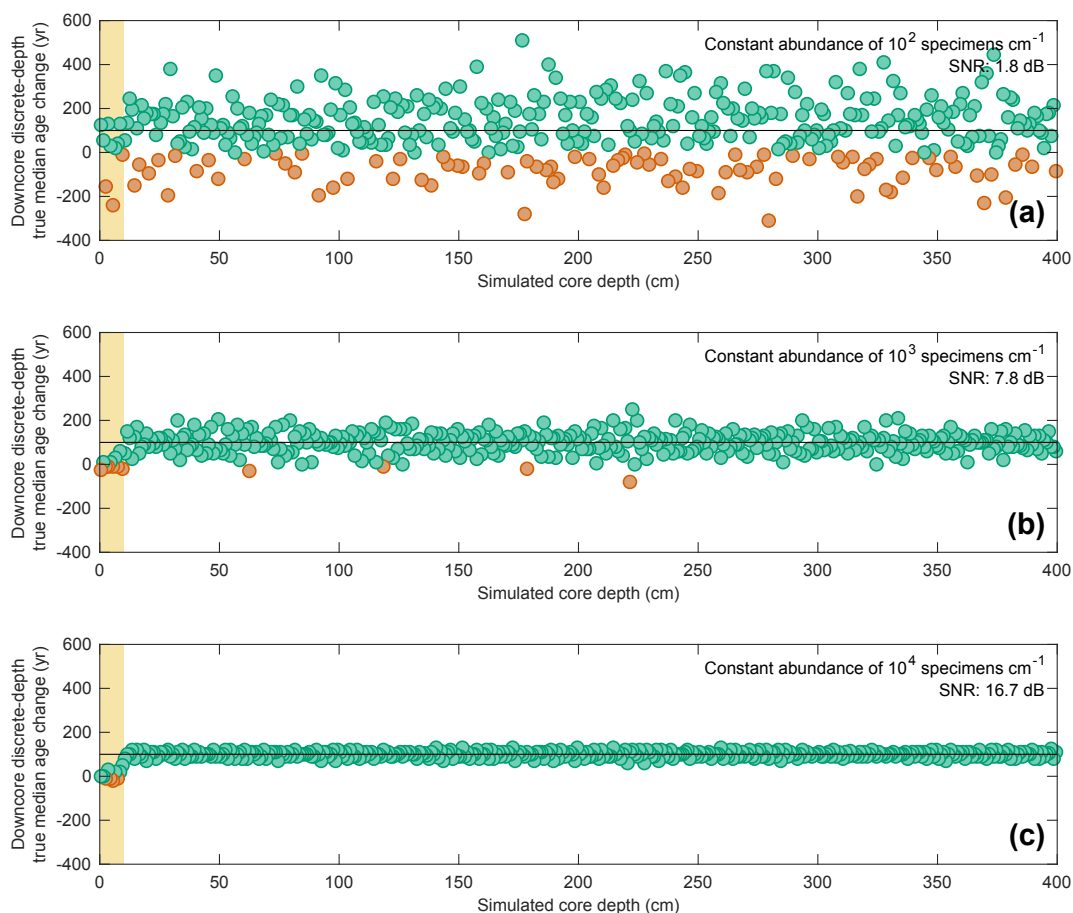


Figure 5. Estimating downcore age-depth noise induced by absolute species abundance in three scenarios all involving involving a constant SAR of 10 cm ka^{-1} and constant bioturbation depth of 10 cm . In all three panels, the data points (circles) indicate the downcore discrete-depth median age increase for each cm of core depth. Green circles correspond to positive downcore median age change, while orange data points correspond to negative downcore median age change (i.e. apparent age reversals). The horizontal black line in each panel denotes the perfect downcore age change of $+100 \text{ years cm}^{-1}$ that would be associated with a constant SAR of 10 cm ka^{-1} . The yellow interval denotes the still-active BD (10 cm) at the core top. The signal-to-noise ratio (SNR) is also computed for each scenario as the ratio between the summed squared magnitudes of the signal and of the noise. The still-active BD at the core top is excluded from the SNR calculation. Three different abundance scenarios are shown: **(a)** constant abundance of 10^2 specimens cm^{-1} . **(b)** constant abundance of 10^3 specimens cm^{-1} . **(c)** constant abundance of 10^4 specimens cm^{-1} .

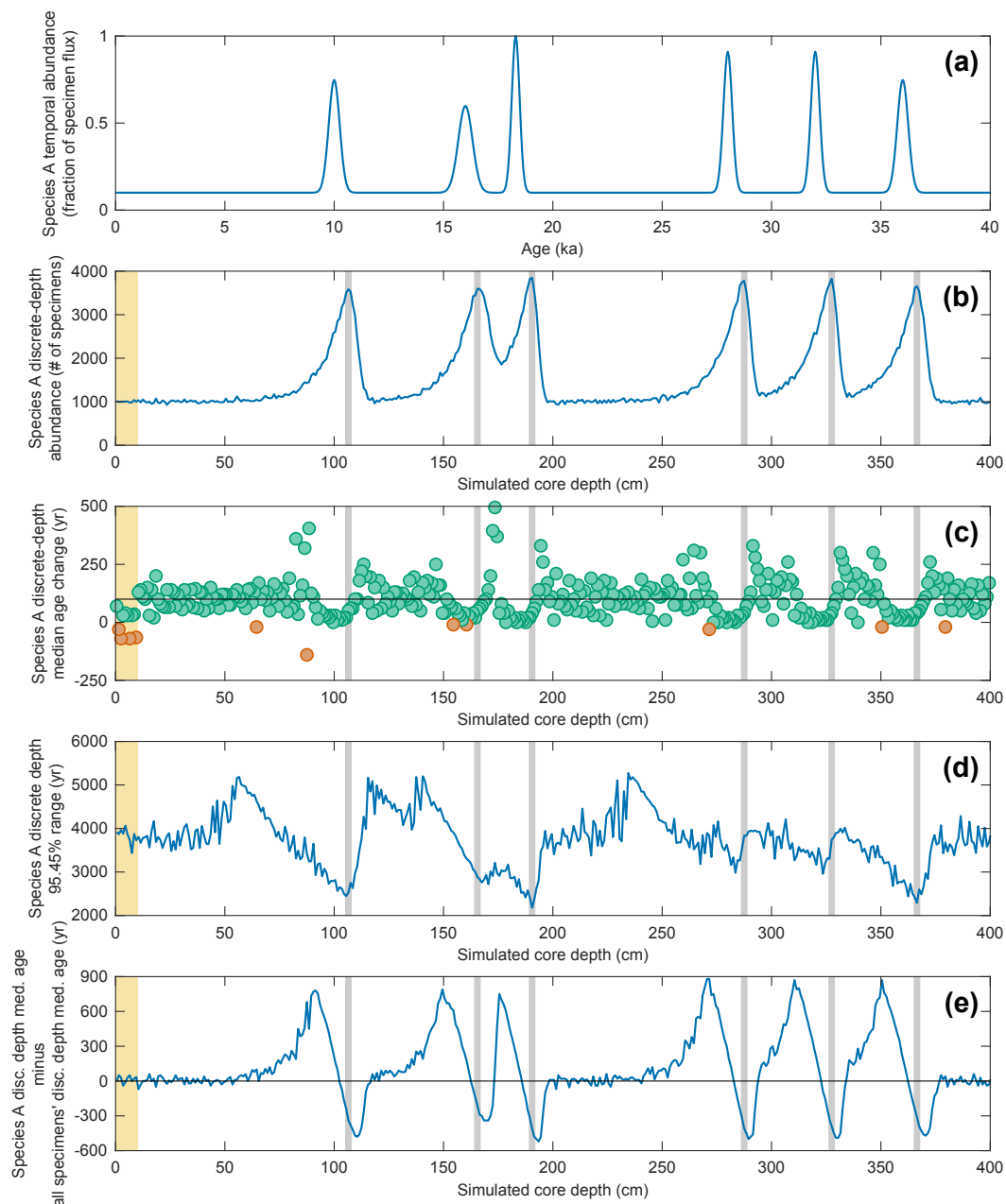


Figure 6. Investigating the effect of temporal changes in a species' abundance upon its discrete-depth age-depth signal in the case of a simulated sediment core with a constant SAR of 10 cm ka and constant BD of 10 cm. In all panels, the yellow interval denotes the still-active BD (10 cm) at the core top. **(a)** The temporal abundance for a given species "Species A" used in the SEAMUS simulation, inputted into the model as a fraction of the per timestep specimen flux. **(b)** The resulting simulated downcore, discrete-depth (1 cm) absolute abundance (number of specimens) for Species A. Vertical grey bands correspond to the depth of the abundance peaks. **(c)** The downcore, discrete-depth (1 cm) change in median age based on samples containing only Species A specimens. Green circles denote downcore increase in discrete-depth apparent median age (i.e. positive apparent SAR) and orange circles denote downcore decrease in discrete-depth median age (i.e. apparent age reversals). The horizontal black line in each panel denotes the perfect downcore age change of +100 years cm⁻¹ that would be associated with a constant SAR of 10 cm ka⁻¹. **(d)** The 95.45% age range of for Species A for each discrete 1 cm depth. **(e)** The offset between the median age of Species A (Med_A) and the